

Calculated optical properties of Co in ZnO: internal and ionization transitions

A. Ciechan^{1,*} and P. Bogusławski^{1,†}

¹*Institute of Physics, Polish Academy of Sciences, al. Lotników 32/46, 02-668 Warsaw, Poland*
(Dated: February 27, 2019)

Previous luminescence and absorption experiments in Co-doped ZnO revealed two ionization and one intrashell transition of $d(\text{Co}^{2+})$ electrons. Those optical properties are analyzed within the generalized gradient approximation to the density functional theory. The two ionization channels involve electron excitations from the two Co^{2+} gap states, the $t_{2\uparrow}$ triplet and the $e_{2\downarrow}$ doublet, to the conduction band. The third possible ionization channel, in which an electron is excited from the valence band to the Co^{2+} level, requires energy in excess of 4 eV, and cannot lead to absorption below the ZnO band gap, contrary to earlier suggestions. We also consider two recombination channels, the direct recombination and a two-step process, in which a photoelectron is captured by Co^{3+} and then recombines via the internal transition. Finally, the observed increase the band gap with the Co concentration is well reproduced by theory.

The accurate description of ZnO:Co is achieved after including $+U$ corrections to the relevant orbitals of Zn, O, and Co. The $+U(\text{Co})$ value was calculated by the linear response approach, and independently was obtained by fitting the calculated transition energies to the optical data. The respective values, 3.4 and 3.0 eV, agree well. Ionization of Co induces large energy shifts of the gap levels, driven by the varying Coulomb coupling between the $d(\text{Co})$ electrons, and by large lattice relaxations around Co ions. In turn, over ~ 1 eV changes of Co^{2+} levels induced by the internal transition are mainly caused by the occupation-dependent $U(\text{Co})$ corrections.

I. INTRODUCTION

ZnO doped with Co is studied since five decades. The detailed experimental investigations conducted by Koidl [1] showed that Co in ZnO substitutes for Zn and acquires the Co^{2+} (d^7) electronic configuration with spin $3/2$. Information about the Co-induced levels was provided by optical measurements. Both internal $d(\text{Co})$ and ionization transitions were observed. The intrashell line at about 2.0 eV originates in the $e_{2\downarrow} \rightarrow t_{2\downarrow}$ (i.e., ${}^4A_2 \rightarrow {}^4T_1$) transition, and typical is fine split [1–12]. The observed splittings, of the order of few tens of eV, are due to a combined effect of the crystal field and the weak spin-orbit coupling, and they are not always experimentally resolved. Next, there are two ionization transitions beginning just below the ZnO band gap [2, 6, 8, 10, 13], which are also reflected in photoconductivity. Those sub-band gap optical transitions can lead to applications in photocatalysis and photovoltaics [14, 15]. The internal excitations of Co^{2+} are utilized in efficient hydrogen production by photoelectrochemical water-splitting [16]. The near UV-visible photodetectors are fabricated with Co-doped ZnO nanoparticles [17, 18].

Investigations of ZnO:Co were intensified by the discovery of ferromagnetism (FM) at room temperatures [19–22]. Mechanism of magnetic coupling depends critically on the sample microscopic morphology [23, 24], and in particular on the presence of defects [19–22, 25]. While the origin of FM in ZnO:Co is out of the scope of this paper, it is obvious that the electronic structure of

Co determines both its charge and spin states as a function of the Fermi energy, thus providing a necessary basis for understanding magnetic coupling between Co ions.

Accurate and efficient theoretical description of transition metal (TM) dopants by first principles methods remains a challenging problem. The underestimation of the single-particle band gap E_{gap} by the local density (LDA) and the generalized gradient (GGA) approximations in the density functional theory distorts the levels, accessible charge states, and ionization energies of TM ions in ZnO. This is the case of electronic structure of Co calculated in Refs [26–28]. An efficient procedure improving the LDA or GGA electronic structure of the host as well as the properties of TM dopants consists in adding the $+U$ terms [29]. Those terms can be treated as adjustable parameters, or can be calculated self-consistently [29], but they should be applied to all orbitals relevant for the problem. For example, in the case of the LDA+ U and GGA+ U calculations in which only the d states of Zn ions are corrected [30–34], the band gap problem persists, and the predicted Co levels are not reliable. Two correction schemes giving a correct band gap of ZnO are the non-local external potential (NLEP) corrections [35, 36] and the self-interaction-corrections (SIC) [37, 38]. The correct E_{gap} of ZnO is also obtained with hybrid functionals (HY) [27, 33, 39, 40]. Linear response time-dependent density functional theory provides excited state energies, and it was recently applied to ZnO:Co [41, 42]. However, the computational cost of those methods is much higher than that of LDA+ U and GGA+ U . The relatively low cost of $+U$ methods is important in the context of high-throughput computations aimed at, e.g., optimization of selected material properties for applications.

Table I summarizes the calculated values of E_{gap} of ZnO and the energies of the three Co^{2+} gap levels. They

* ciechan@ifpan.edu.pl

† bogus@ifpan.edu.pl

TABLE I. Calculated ZnO band gap and energies of the Co^{2+} levels. The symbol “ \sim VBM” denotes the cases when the majority spin states are close to the VBM, or are degenerate with the valence bands. Several values are inferred from the figures showing density of states, and thus they are of limited accuracy. All values are in eV.

Ref.	method	E_{gap}	$t_{2\uparrow}$	$e_{2\downarrow}$	$t_{2\downarrow}$	comments
[26]	LDA	< 2	\sim VBM	1.0	2.2	
[27]	GGA	0.8	\sim VBM	0.8	2.0	
[28]	GGA	1.2	0.3	1.3	3.0	
[30]	LDA+ U	0.8	\sim VBM	1.0	4.0	$U(\text{Zn}) = 0, U(\text{Co}) = 4.0$ eV
[32]	LDA+ U	2.0	\sim VBM	0.1	4.0	$U(\text{Zn}) = 9.0$ eV, $U(\text{Co}) = 5.0$ eV
[33]	GGA+ U	1.6	\sim VBM	1.2	3.3	$U(\text{Zn}) = 7.0$ eV, $U(\text{Co}) = 2.0$ eV
[35]	GGA+ U + NLEP	3.3	\sim VBM	0.8	4.5	$U(\text{Zn}) = 2.8$ eV, $U(\text{Co}) = 7.0$ eV
[37]	SIC	3.0	\sim VBM	1.0	3.5	
[38]	SIC	3.0	0.5	1.0	4.0	
[39]	HY	3.3	\sim VBM	0.8	6.0	
[40]	HY	4.5	\sim VBM	0.5	6.0	results for quantum dot $(\text{Zn}_{140}\text{Co})\text{O}_{141}$
[27]	HY	3.4	\sim VBM	1.5	5.0	
[33]	HY+ GW_0	3.3	\sim VBM	0.8	7.1	
present	LDA+ U	3.3	0.3	1.3	5.0	$U(\text{Zn}) = 12.5$ eV, $U(\text{O}) = 6.25$ eV, $U(\text{Co}) = 3.0$ eV
	LDA+ U	3.3	\sim VBM	0.9	5.2	$U(\text{Zn}) = 12.5$ eV, $U(\text{O}) = 6.25$ eV, $U(\text{Co}) = 4.0$ eV

are qualitatively similar, predicting the majority-spin levels close to the valence band maximum (VBM), the minority $e_{2\downarrow}$ level in the lower half of the band gap, and the crystal field splitted $t_{2\downarrow}$ level higher in energy. Quantitatively, however, the discrepancy between various methods exceeds 4 eV, which is only partially explained by the large band gap error of the LDA and GGA. Indeed, even the corrected approaches, such as SIC or LDA+ U , lead to differences larger by more than 1 eV.

Correctness of a theoretical approach is assessed by comparing the results of calculations to experiment. This issue was not discussed in the quoted works, except Refs [40–42]. In the case of ZnO:Co, experiment includes optical, transport, and magnetic measurements, and the corresponding observables are optical transition energies, thermal ionization energies, and magnetic moments and couplings. Importantly, energies of excited states cannot be inferred from the differences in one-electron energies because of the strong intrashell coupling of $d(\text{Co})$ electrons, large lattice relaxations induced by the change of the Co charge state, and the presence of non-negligible (albeit small in ZnO) electron-hole coupling. A striking example is that of the internal $d(\text{Co})$ excitation: its experimental energy is 2.0 eV, while the $e_{2\downarrow}$ - $t_{2\downarrow}$ energy difference obtained with hybrid functionals is more than twice higher, see Table I. This feature is also important when analyzing ionization (charge transfer) transitions, since the Co levels are sensitive to its charge state, and thus the calculations should be extended to charged Co. This was performed in Refs [34, 36] which calculated the transition levels.

The aim of this paper is to provide a theoretical interpretation of the measured optical properties of ZnO:Co. To this end, we focus on the relevant transition ener-

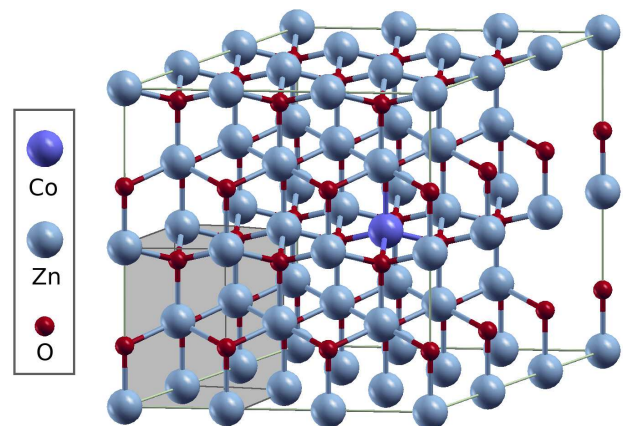


FIG. 1. $3 \times 3 \times 2$ supercell of ZnO with Co impurity. Shaded region indicates a single unit cell of pure ZnO with 4 atoms.

gies rather than one electron levels. We also consider the change of the band gap of ZnO induced by Co. The paper is organized as follows. In Section II, we present the method of calculations, including the calculations of the $U(\text{Co})$ term. The results of the electronic structure and optical transitions of ZnO:Co are shown in Section III A and III B. The comparison of calculated results with experiment and their interpretation, given in Section III C, allow to find the optimal value of $U(\text{Co})$. Section IV summarizes the obtained results.

II. CALCULATION DETAILS

The calculations are performed within the density functional theory in the GGA approximation of the exchange-correlation potential [43–45], supplemented by the $+U$ corrections [29, 46, 47]. We use the pseudopotential method implemented in the QUANTUM ESPRESSO code [48], with the valence atomic configuration $3d^{10}4s^2$ for Zn, $2s^2p^4$ for O and $4s^2p^03d^7$ for Co. The plane-waves kinetic energy cutoffs of 30 Ry for wavefunctions and 180 Ry for charge density are employed. Spin-orbit coupling is neglected.

The electronic structure of the wurtzite ZnO is examined with a $8 \times 8 \times 8$ k -point grid. Analysis of the Co impurity is performed using $3 \times 3 \times 2$ supercells with 72 atoms shown in Fig. 1, and the k -space summations performed with a $3 \times 3 \times 3$ k -point grid. Larger supercells ($3 \times 3 \times 4$ with 144 atoms) and smaller supercells ($2 \times 2 \times 2$ with 32 atoms and $2 \times 2 \times 1$ with 16 atoms) are employed to obtain the dependence of the energy gap on the Co concentration. The ionic positions of ZnO:Co are optimized until the forces acting on ions became smaller than 0.02 eV/Å. The calculated lattice constants of ZnO, $a = 3.23$ Å and $c = 5.19$ Å, as well as internal parameter $u = 0.38$, are underestimated by less than 1 % in comparison with experimental values [49, 50]. The calculated average Co-O bond lengths for Co^{2+} are 1.99 Å, close to those of Zn-O, 1.97 Å.

The underestimation of the band gap of ZnO is corrected by applying the U term to $d(\text{Zn})$ and $p(\text{O})$ electrons. We find that the corrections $U(\text{Zn}) = 12.5$ eV and $U(\text{O}) = 6.25$ eV reproduce not only the experimental ZnO gap of 3.3 eV [51–53], but also the width of 6 eV of the upper valence band of mostly $2p(\text{O})$ character, and the energy of the $d(\text{Zn})$ band, centered about 8 eV below the VBM [54]. Those values of the U terms were tested by us for ZnO:Mn and ZnO:Fe [55, 56]. $U(\text{O})$ directly opens the gap since the VBM is mainly derived from the $p(\text{O})$ orbitals, while $U(\text{Zn})$ changes the position of the $d(\text{Zn})$ -derived band well below the VBM. In previous works [57, 58], $U(\text{Zn}) = 10 - 12$ eV and $U(\text{O}) = 6 - 7$ eV were proposed, while in Ref. [59] $U(\text{Zn}) = 12.8$ eV and $U(\text{O}) = 5.29$ eV were calculated by using pseudohybrid Hubbard density functional method. This consistency between the results of various approaches provides a complementary justification for our $+U$ values. Finally, we mention that by the band gap E_{gap} we understand the single-particle band gap, which is equal to the energy difference between the Kohn-Sham energies of the conduction band minimum (CBM) and the VBM. As it was discussed in Ref. [60], this also corresponds to the quasi-particle band gap. Inclusion of excitonic effects would be necessary in a detailed study of the optical response of ZnO, but this problem is outside the scope of this work.

The calculated total energies for all the considered charge states are used to obtain the transition levels $\varepsilon(q/q')$ between various charge states of Co. In the case of charged supercells, the image charge corrections and

potential alignment are included in the calculations according to [60, 61].

The value of the U correction for $d(\text{Co})$ is obtained in two ways. First, it is considered as a free parameter varying from 0 to 6 eV. The best agreement with the experimental optical transition energies is obtained for $U(\text{Co}) = 3$ eV. Second, we also compute $U(\text{Co})$ by linear response approach proposed in Ref. [29]. We add small potential shifts that act only on the localized d orbitals of Co through a projection operator, $\Delta V = \alpha \sum_m |\phi_m\rangle\langle\phi_m|$, and calculate variation of the Co occupations. The obtained (interacting and noninteracting) density response functions of the system with respect to these perturbations are used to compute the $U(\text{Co})$ term. In the above procedure, we use a supercell with 72 atoms and then extrapolate the results to larger supercell with over 300 Co ions. We obtain $U(\text{Co}) = 3.4$ eV, which is a little higher than the value fitted to experiment. Importantly, the constrained calculations with fixed initial occupations of $d(\text{Co})$ orbitals are needed, because final total energies depend on the initial fixed on-site occupation matrices. Therefore, we test all possible occupations of Co orbitals with integer occupation numbers 0 and 1 to find the state with minimum energy for a given charge state q .

To find energies of optical transitions of Co in ZnO two approaches are used. The ionization energy for the transition $\text{Co}^{2+} \rightarrow \text{Co}^{3+}$ is obtained from the energy of $\varepsilon(+/0)$ level relative to the CBM, while that for $\text{Co}^{2+} \rightarrow \text{Co}^{1+}$ is obtained from the energy of $\varepsilon(0/-)$ relative to the VBM. A second approach is used to find energies of the excited configurations (obtained after e.g. the internal transition from Co^{2+} to the excited $(\text{Co}^{2+})^*$ state). In this case, the occupations of the Kohn-Sham levels are fixed, and the Brillouin zone summations are approximated by the Γ point values [48]. Moreover, supercells remain electrically neutral even when the ionized Co^{3+} is analyzed because of the presence of the excited electron in the conduction band. In consequence, the electric fields generated by Co^{3+} are largely screened, their impact on both excitation energies and the Co gap levels [62] is expected to be small, and total energies need not to be corrected for the spurious defect-defect coupling. These two approaches give ionization energies that agree to within less than 0.1 eV.

III. RESULTS

A. Co levels in ZnO

Figure 2(a) shows the band structure and the density of states (DOS) of ZnO doped with Co^{2+} for $U(\text{Co}) = 0$. Co^{2+} introduces three levels in the gap: close-lying $e_{2\uparrow}$ doublet and $t_{2\uparrow}$ triplet at about 1.5 eV above the VBM, and the $e_{2\downarrow}$ doublet at 3.2 eV. The empty triplet $t_{2\downarrow}$ is degenerate with the conduction band. Actually, both $t_{2\uparrow}$ and $t_{2\downarrow}$ triplets are weakly split by about 0.1 eV by the

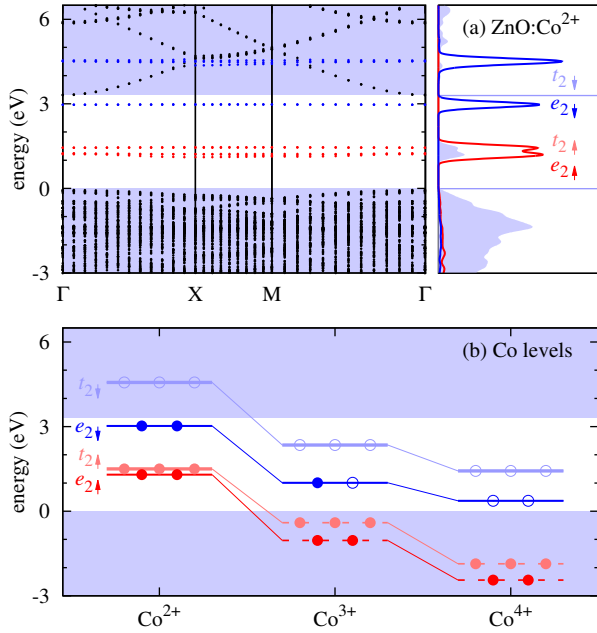


FIG. 2. (a) Band structure (left panel) and DOS (right panel) of ZnO:Co²⁺. Zero energy is at the VBM. Gray areas display the total DOS, while red and blue lines indicate the DOS projected on $d_{\uparrow}(\text{Co})$ and $d_{\downarrow}(\text{Co})$ orbitals, respectively. (b) Kohn-Sham levels of Co in various charge states. Horizontal (gray) lines denote the band gap of ZnO. Electrons and holes on the $d(\text{Co})$ levels are denoted by filled and empty dots, respectively. Spin-up states of Co³⁺ and Co⁴⁺ are smeared out over the valence bands. The calculations are performed for $U(\text{Co}) = 0$.

wurtzite crystal field, but we omit this effect for the sake of clarity. The strong dependence of the Kohn-Sham levels of Co on the charge state is clearly visible in Fig. 2(b). The levels of Co²⁺ with seven d electrons are 1-2 eV higher in energy than those of Co³⁺ with 6 electrons, because the intrashell Coulomb repulsion increases with the increasing d -shell occupation [55, 56, 63]. In particular, the spin-up states of Co³⁺ are below the VBM, while both spin-down levels are in the gap: $e_{2\downarrow}$ at 1.1 eV and $t_{2\downarrow}$ at 2.4 eV above the VBM. The second ionization to Co⁴⁺ farther decreases the Co levels.

The dependence of Co²⁺ and Co³⁺ levels on $U(\text{Co})$ is presented in Fig. 3(a) and 3(b), respectively. The U -induced contribution V_U to the Kohn-Sham potential is [29]

$$V_U |\psi_{k\nu}^{\sigma}\rangle = U \sum_{m,\sigma} (1/2 - \lambda_m^{\sigma}) |\phi_m\rangle \langle \phi_m | \psi_{k\nu}^{\sigma}\rangle, \quad (1)$$

where ϕ_m are the localized d orbitals occupied by λ_m electrons, and $\psi_{k\nu}^{\sigma}$ are the Kohn-Sham states for the wavevector k , band ν , and spin σ . The V_U potential only acts on the contribution of the m th $d(\text{Co})$ orbital to the given (ν, k, σ) state, and this contribution is evaluated by the appropriate projection according to Eq. 1. Equation 1

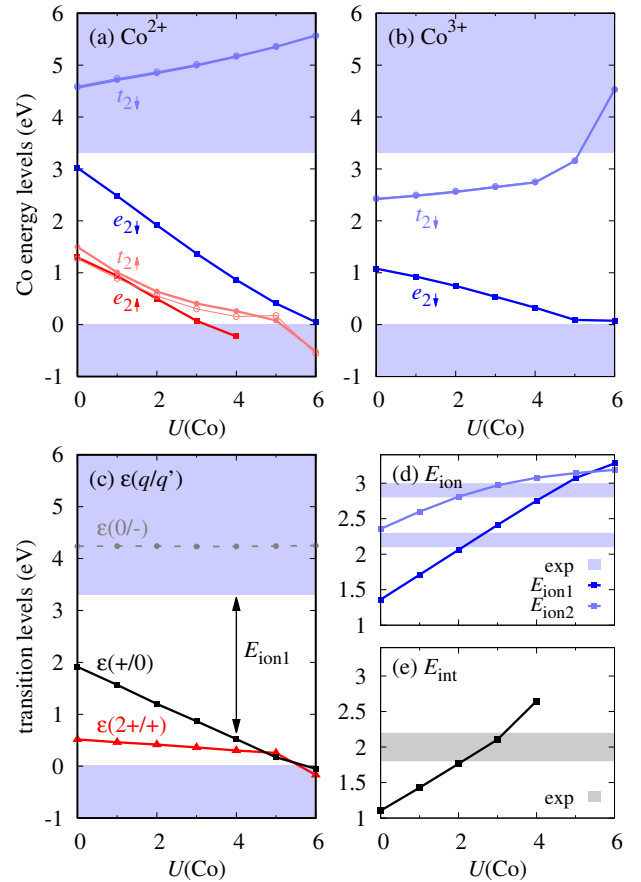


FIG. 3. The Kohn-Sham energy levels of (a) Co²⁺, (b) Co³⁺ and (c) the transition levels $\epsilon(q/q')$ calculated as a function of $U(\text{Co})$. The $\epsilon(0/-)$ is only estimated, see in text for details. The $U(\text{Co})$ dependence of (d) ionization and (e) internal transition energies. Experimental results are shown in both cases: thresholds of ionization transitions are taken from photocurrent measurements [13, 64–66], while the energy range of internal transitions is taken from absorption [1, 3, 5, 8, 9, 11, 12]. See text for definitions of ionization E_{ion1} and E_{ion2} and internal transition E_{int} energies.

also shows that there is a negative shift of the fully occupied $e_{2\uparrow}$, $t_{2\uparrow}$ and $e_{2\downarrow}$ levels of Co²⁺, while the shift is positive for empty $t_{2\downarrow}$. For $U > 4$ eV, the spin-up Co²⁺ levels merge with the valence band. The energy levels of Co¹⁺ are not shown because this charge state is not stable and it will not be assumed by Co for realistic Fermi energies. Indeed, the $t_{2\downarrow}$ of Co²⁺ is at least 1 eV above the CBM, see Fig. 3(a). We note that the exact energy of $t_{2\downarrow}$ relative to the CBM is of importance for the magnetic coupling between Co ions mediated by free carriers, see the discussion in Ref. [67].

The calculated Co²⁺ energy levels are compared with the previous calculations in Table I. The LDA and GGA approximations lead to the underestimated E_{gap} and, in consequence, to the $e_{2\downarrow}$ and $t_{2\downarrow}$ levels degenerate with the conduction band [26–28, 30]. The $U(\text{Co})$ term shifts

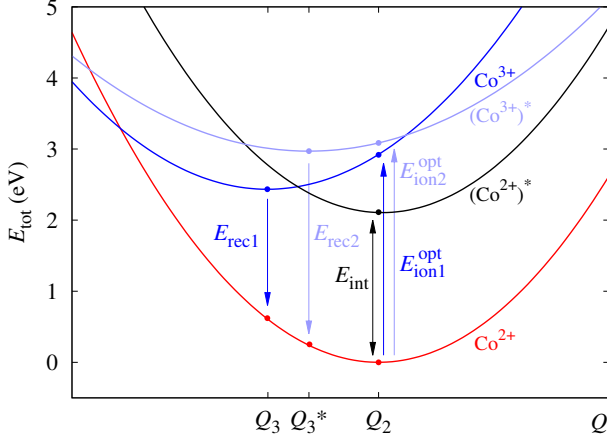


FIG. 4. Total energy change of the Co^{2+} and of the excited states of Co as a function of configuration coordinate Q . Co^{3+} means (Co^{3+}, e_{CB}) , while $(\text{Co}^{3+})^*$ means $((\text{Co}^{3+})^*, e_{CB})$ state. Q_2 , Q_3 and Q_3^* are equilibrium atomic configurations of Co^{2+} , Co^{3+} and $(\text{Co}^{3+})^*$ charge states, associated with Co-O bond lengths. $U(\text{Co}) = 3$ eV is assumed. Ionization and recombination energies are defined in the text.

down all the occupied Co levels, and thus the $e_{2\downarrow}$ is in the band gap [32, 33], as in our case. However, ionization energies are too low since the gap is strongly underestimated even if $U(\text{Zn})$ is applied [32, 33]. On the other hand, our results obtained with $U(\text{Co}) = 3 - 4$ eV are in a reasonable agreement with bandgap corrected methods employed in Refs [27, 33, 35, 37–40], and in particular with the HY calculations.

The dependence of the Co levels on $U(\text{Co})$ is reflected in the corresponding dependence of the thermodynamic transition levels shown in Fig. 3(c). The value of $\varepsilon(0/-)$ given in Fig. 3(c) is only estimated, since the $t_{2\downarrow}$ electron of Co^{1+} would autoionize to the CBM. In turn, the $\varepsilon(+/0)$ and $\varepsilon(2+/+)$ levels are in the gap, indicating that Co^{2+} , Co^{3+} and Co^{4+} are possible stable charge states of Co in ZnO. Transition levels $\varepsilon(+/0) = 0.85$ eV and $\varepsilon(0/-) = 4.5$ eV (i.e., 1.1 eV above the CBM) were obtained in Ref [34], and $\varepsilon(+/0) = 0.4$ eV and $\varepsilon(0/-) = 3.7$ eV (i.e., 0.9 eV above the CBM) in Ref [36]. Our results for $U(\text{Co}) = 3 - 4$ eV are between those of Ref. [34] and Ref. [36]. The $\varepsilon(2+/+)$ transition level, which was not considered in Refs [34, 36], is practically degenerate with the VBM.

B. Optical transitions

We consider four optical excitation processes, namely three ionization channels and the internal excitation, together with the corresponding recombination transitions. We also study the composition dependence of the E_{gap} . Figure 4 shows the configuration diagram, where the configuration coordinate Q should be regarded as the aver-

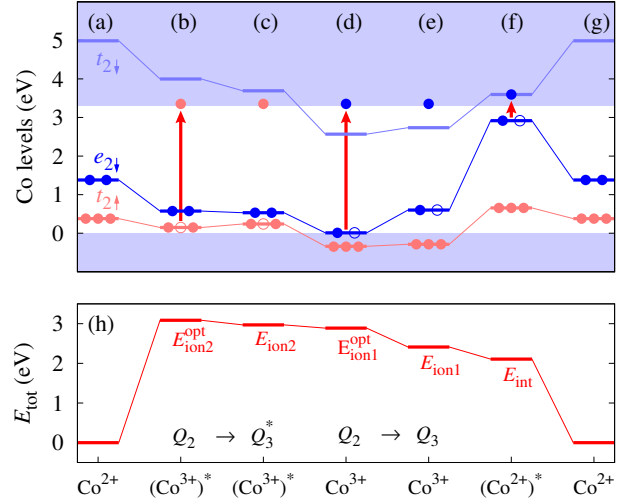
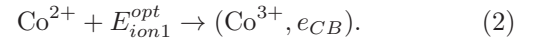


FIG. 5. (a-g) The changes of $t_{2\uparrow}$, $e_{2\downarrow}$ and $t_{2\downarrow}$ levels induced by the ionization and intrashell transitions. The levels of Co at Q_2 correspond to vertical transitions, while these ones at Q_3 and Q_3^* include relaxation of Co^{3+} and $(\text{Co}^{3+})^*$ to their equilibrium configurations. Total energies relative to that of Co^{2+} are shown in panel (h). $U(\text{Co}) = 3$ eV is assumed.

age Co-O bond length for a given electronic configuration of Co. The involved systems are Co^{2+} , its excited state $(\text{Co}^{2+})^*$, as well as Co^{3+} and its excited $(\text{Co}^{3+})^*$ state. The corresponding equilibrium configuration coordinates are Q_2 , Q_2^* , Q_3 , and Q_3^* . $U(\text{Co}) = 3$ eV is assumed.

1. The first ionization channel consists in the vertical optical ionization of Co^{2+} with the energy E_{ion1}^{opt} , when an electron is transferred from the $e_{2\downarrow}$ level to the CBM,



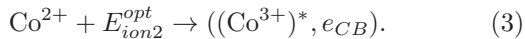
During calculations for this process, the occupation of the initial state is fixed to be $(e_{2\uparrow}^2 t_{2\uparrow}^3 e_{2\downarrow}^2 t_{2\downarrow}^0)$, while that of the final state is $(e_{2\uparrow}^2 t_{2\uparrow}^3 e_{2\downarrow}^1 t_{2\downarrow}^0, e_{CB})$, see also Fig. 5(a), Fig. 5(d-e), and Fig. 4. The calculated optical ionization energy E_{ion1}^{opt} of the vertical transition is 2.9 eV. After the excitation, the system can relax from the equilibrium configuration Q_2 of Co^{2+} toward that of Co^{3+} , Q_3 , which lowers the total energy by 0.5 eV. Thus, the onset of the absorption is predicted to occur at the zero phonon line energy $E_{ion1} = 2.4$ eV.

The change of the charge state causes the reduction of Co-O bonds by about 5 per cent, which is reflected in the difference between Q_2 and Q_3 in Fig. 4. The photoelectron recombines $[(\text{Co}^{3+}, e_{CB}) \rightarrow \text{Co}^{2+}]$ with the recombination energy E_{rec1} . The energy E_{rec1} of Co^{3+} at equilibrium is 1.8 eV. After recombination, the system relaxes to Q_2 releasing 0.6 eV.

Experimentally, luminescence energies are affected by the ratio of the radiative recombination rate to the lattice relaxation time of phonon emission. When the recombination is fast, the system does not relax to equilibrium,

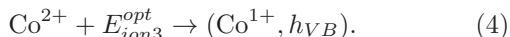
and the absorption and emission energies are almost equal to each other. In the opposite limit, long recombination times allow for the full relaxation of atomic configurations by phonon emission, which increases the difference between E_{ion1}^{opt} and E_{rec1} , i.e., the Franck-Condon shift.

2. The second ionization channel consists in the ionization of Co^{2+} via electron transfer from $t_{2\uparrow}$ to the CBM:



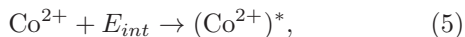
The occupations in the excited state $(\text{Co}^{3+})^*$ are $(e_{2\uparrow}^2 t_{2\uparrow}^2 e_{2\downarrow}^2 t_{2\downarrow}^0, e_{CB})$, as indicated in Fig. 5(b-c). The corresponding ionization and recombination energies are E_{ion2}^{opt} and E_{rec2} . Ionization of Co^{2+} to $(\text{Co}^{3+})^*$ produces a ~ 3 per cent shortening of Co-O bonds, which is smaller than in the case of Co^{3+} . For this reason, the relaxation energy is smaller, about 0.1 eV, and the vertical and zero phonon absorption energies are similar, $E_{ion2}^{opt} = 3.1$ eV and $E_{ion2} = 3.0$ eV, respectively. The Franck-Condon shift between absorption and emission lines is also smaller since the recombination energy at the configuration Q_3^* is $E_{rec2} = 2.7$ eV.

3. The third possible ionization channel consists in the ionization of Co^{2+} when an electron is transferred from the VBM to $t_{2\downarrow}$ leaving a hole in the valence band, h_{VB} :



In that case, fixed occupations for ionized state are $(h_{VB}, e_{2\uparrow}^2 t_{2\uparrow}^3 e_{2\downarrow}^2 t_{2\downarrow}^1)$. As it was pointed out above and shown in Fig. 3(c), the transition level $\varepsilon(0/-)$ lies above the CBM, and thus the Co^{1+} charge state is not stable. The photoionization energy E_{ion3} is above 4 eV, higher than E_{gap} .

4. The internal excitation of Co^{2+} ,



consists in the transfer of an electron from the doubly occupied $e_{2\downarrow}$ to the empty $t_{2\downarrow}$ level, thus $(e_{2\uparrow}^2 t_{2\uparrow}^3 e_{2\downarrow}^1 t_{2\downarrow}^1)$ is fixed for $(\text{Co}^{2+})^*$ as shown in Fig. 5(f). The corresponding excitation energy is denoted by E_{int} , and we find $E_{int} = 2.1$ eV. In this case, $Q_2 \approx Q_2^*$, since the charge state of the dopant remains unchanged and the redistribution of $d(\text{Co})$ electrons affects the bonds by less than 0.1%.

A further insight into those processes can be gained from Fig. 5, which shows the $t_{2\uparrow}$, $e_{2\downarrow}$ and $t_{2\downarrow}$ levels calculated for six cases: Co^{2+} at equilibrium Q_2 (panels (a) and (g)), the photoionized $((\text{Co}^{3+})^*, e_{CB})$ at the Q_2 and Q_3^* configurations (panels (b) and (c)), the (Co^{3+}, e_{CB}) at Q_2 and Q_3 (panels (d) and (e)), and finally the $(\text{Co}^{2+})^*$ state at Q_2 (panel (f)). The excited states are ordered from the highest to the lowest total energies, which are given in panel (h). The dependence of the Kohn-Sham levels of Co on the charge state follows from two effects. The first and the dominant one is the

reduced Coulomb intrashell repulsion characterizing the ionized Co^{3+} and $(\text{Co}^{3+})^*$, which induces downward shift of gap levels relative to those of the neutral Co^{2+} . The second effect is the upward shift of the energies of Co levels, which are induced by the decrease of Co-O bond lengths from Q_2 to Q_3 or Q_3^* , see also Ref. [55]. Both effects are stronger for Co^{3+} , where the optical ionization decreases the position of Co levels by 1.5 eV, while the relaxation from Q_2 to Q_3 rises the Co levels by ~ 0.7 eV. The changes induced by the internal transition, shown in the panels (g)-(f), have a different origin. In this case, the energy shifts of $e_{2\downarrow}$ and $t_{2\downarrow}$ are comparable, and are caused mainly by the $U(\text{Co})$ correction. They have opposite signs because, in agreement with Eq. 1, after the excitation from Co^{2+} to $(\text{Co}^{2+})^*$, the occupation of $t_{2\downarrow}$ increases by 1 and that of $e_{2\downarrow}$ decreases by 1.

Considering recombination processes we see that after the internal excitation of Co^{2+} , the $t_{2\downarrow}$ occupied with one electron is about 0.25 eV above the CBM. This suggests that the excited $(\text{Co}^{2+})^*$ can spontaneously ionize, releasing one electron to the CBM in the reaction $[(\text{Co}^{2+})^* \rightarrow (\text{Co}^{3+}, e_{CB})]$, i.e., a transition from (f) to (e) should spontaneously occur. However, the total energy of the latter state is 0.3 eV *higher* than the energy of $(\text{Co}^{2+})^*$, see Fig. 5(h), and therefore the ionization is possible, but it is a thermally activated process. Second, the results of Fig. 4 show that there are two possible channels of recombination for Co^{3+} and $(\text{Co}^{3+})^*$. The first one is the one-step direct recombination with E_{rec1} or E_{rec2} , while the second channel is a two-step process, in which the electron capture on $t_{2\downarrow}$ or $e_{2\uparrow}$ is followed by the internal deexcitation.

The above results illustrate the fact that excitation energies cannot be estimated based on the single-electron energies. In particular, the calculated internal transition energy is 2.1 eV, while the energy difference between the Co^{2+} levels is almost twice larger, 3.5 eV. Such a large discrepancy is expected to hold also for hybrid functionals calculations [27, 33, 39, 40].

Comparing our results with the recent study in Ref. [42] using the linear response time dependent density functional theory, we note that their results for the excitation to $(\text{Co}^{2+})^*$ and Co^{3+} states were obtained for small quantum dots and extrapolated to bulk ZnO, nevertheless they agree with our values to within 0.2 eV.

5. Finally, the observed optical properties of ZnO:Co include also fundamental excitation and recombination transitions with energy given by the band gap. As it is shown in Fig. 6, the calculated E_{gap} increases with the increasing Co concentration. The detailed analysis of those transitions must include formation of excitons (which binding energy in ZnO is 60 meV [68]), but this issue is out of the scope of this work.

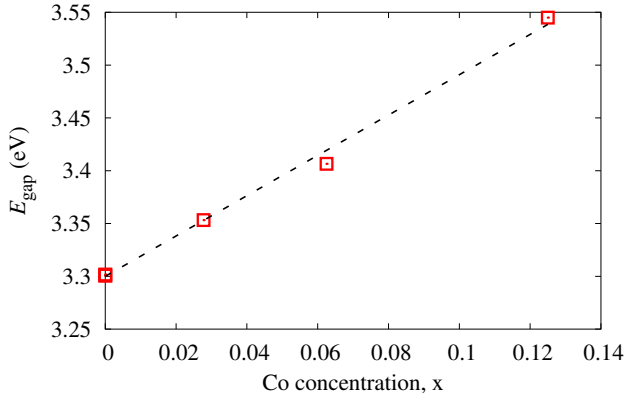


FIG. 6. The Kohn-Sham band gap as a function of Co concentration in $Zn_{1-x}Co_xO$. $U(Co) = 3$ eV is assumed. Squares denote supracell results, and the dashed line shows the fitted dependence $E_{gap}(x) = E_{gap}(0) + bx$, with $E_{gap}(0) = 3.3$ eV and $b = 1.9$ eV.

C. Comparison with experiment

The comparison of our results with the experimental data is satisfactory. The calculated dependencies of E_{ion} and E_{int} on $U(Co)$ allow to find its optimal value. The results are shown in Fig. 3(d) and (e). A good agreement with experiment is obtained with $U(Co) = 3.0$ eV. In particular:

(i) The observed increase of the band gap with the Co concentration x is well reproduced, see Fig. 6. The calculated coefficient b defined by the relation $E_{gap}(x) = E_{gap}(0) + bx$ is 1.9 eV, which agrees well with the experimental values 1.1 [3], 1.7 [4], 2.3 [66] and 2.5 eV [9].

(ii) Our energy of the internal transition $E_{int} = 2.1$ eV is close to the experimental ~ 2.0 eV, which is seen in both absorption and luminescence. The observed splitting of this line is partly due to the crystal field splitting of the $t_{2\downarrow}$ level, and partly due to the spin-orbit coupling, which is neglected in our calculations [69].

(iii) The optical ionization of Co^{2+} is observed in a broad band which begins at about 2.2 eV, extends up to about 3 eV, and was monitored in photocurrent by Gamelin *et al.* [13, 64–66]. Their further analysis revealed that it originates in two transitions, the lower energy one assigned to $[Co^{2+} \rightarrow (Co^{3+}, e_{CB})]$, and the higher energy transition interpreted as $[Co^{2+} \rightarrow (Co^{1+}, h_{VB})]$.

According to our results, the ionization energy corresponding to the zero-phonon transition $[Co^{2+} \rightarrow (Co^{3+}, e_{CB})]$ is about 2.4 eV, and the phonon-assisted transitions extend up to $E_{ion1}^{opt} = 2.9$ eV. Both values are higher by about 0.2 eV relative to experiment. This reasonable agreement confirms the assignment proposed in Refs [13, 64–66]. This 2.4-2.9 eV absorption band is shown in Fig. 7(a). Its width can also be inferred from Fig. 4.

On the other hand, the obtained results do not support the identification of the second ionization tran-

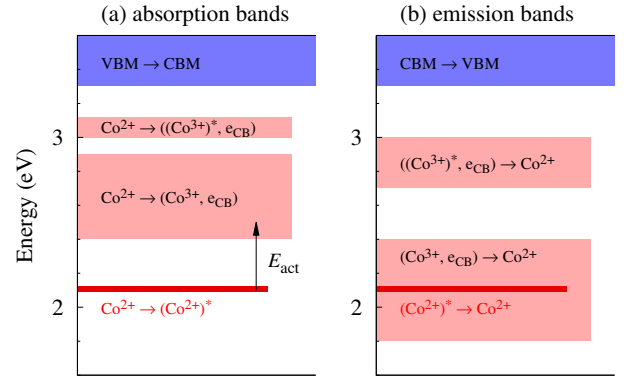


FIG. 7. Calculated (a) absorption and (b) emission bands.

sition as $[(Co^{2+}) \rightarrow (Co^+, h_{VB})]$, in which an electron is excited from the VBM to Co^{2+} level at energies above 2.7 eV [13, 64–66]. Indeed, our results show that this transition requires at least 4 eV, as it follows from the energy of the $\epsilon(0/-)$ transition level relative to the VBM (see Fig. 3(c)). Instead, we propose that the observed higher absorption band originates in $[(Co^{2+}) \rightarrow ((Co^{3+})^*, e_{CB})]$ transition from the Co spin-up state with the ionization energy in the range 3.0-3.1 eV shown in Fig. 7(a).

In the absorption measurements, only one ionization channel is seen at energies just below the band gap [2, 4, 6, 9, 10]. Based on our results, we assign this transition to $t_{2\uparrow} \rightarrow CBM$, *i.e.* to $[Co^{2+} \rightarrow (Co^{3+})^*, e_{CB}]$, because its energy fits the experiment. Moreover, the second possible transition, $e_{2\downarrow} \rightarrow CBM$, is expected to be forbidden.

(iv) According to our results, after the internal excitation $(Co^{2+})^*$ can ionize releasing an electron to the CBM, and the corresponding activation energy is $E_{act} = 0.3$ eV. The experiments of Refs [64–66] revealed that $(Co^{2+})^*$ indeed ionizes, because the internal transition results in photoconductivity. The observed ionization has a thermally activated character with energy of about 50 meV, which is somewhat smaller than the calculated value.

The calculated absorption and emission bands are summarized in Fig. 7. The lowest energy excitation at 2.1 eV is associated with the internal transition to excited Co^{2+} . Next, the two sub-bands corresponding the ionization transitions from Co^{2+} to Co^{3+} and $(Co^{3+})^*$ appear at 2.4-2.9 eV and at 3.0-3.1 eV. Each subband extends from the zero-phonon transition at energy $E_{ion1(2)}$ (which includes atomic relaxations around Co) to the line at $E_{ion1(2)}^{opt}$ of the vertical transition (*i.e.*, without changes in atomic positions). At the highest energies, above 3.3 eV, the VBM \rightarrow CBM transitions occurs. The energy range of charge transfer and ZnO band-to-band transitions are expected to change with the Co concentration. In the emission bands, the transitions from Co^{3+} and $(Co^{3+})^*$ to Co^{2+} occur at 1.8-2.4 eV and 2.7-3.0 eV, respectively. Here again, the finite width of subbands spans the en-

ergy window between the zero-phonon lines $E_{ion1(2)}$ and the vertical transitions $E_{rec1(2)}$. (The widths of both absorption and emission bands can be inferred from Fig. 4, where the vertical transitions are shown by arrows.) Both transitions can be completely suppressed by the two step processes involving $(Co^{2+})^*$, which is probably observed in the luminescence [7, 9, 11, 12, 70].

IV. CONCLUSIONS

The results of the GGA+ U calculations explain the available experimental properties of substitutional Co in ZnO. In particular, the calculated composition dependence of the ZnO:Co band gap agrees well with the experimental data [3, 4, 9, 66]. While the n-doping of ZnO:Co does not change the charge state of Co, the p-doping will be compensated because Co can act as a double donor.

We considered four possible optical transitions involving Co^{2+} . The first one is the internal $d-d$ transition, which calculated transition energy, 2.1 eV, corresponds well with the experimental value 2.0 eV. Next, there are two ionization transitions $Co^{2+} \rightarrow Co^{3+}$, in which an electron is transferred from one of the two $d(Co)$ gap states to the conduction band. The lower energy channel is related with the excitation from $e_{2\downarrow}$ to CBM, with energies in the range 2.9-2.4 eV, in which the upper limit corresponds the zero phonon line. The higher energy channel is related with the transition $t_{2\uparrow} \rightarrow CBM$ with energies 3.1-3.0 eV, and leaving Co in the excited state $(Co^{3+})^*$. Both excitation channels occur in parallel, and extent from 3.1 eV to 2.4 eV. This agrees to within 0.2 eV with observations. The fourth possible ionization process consists in exciting an electron from the valence band to the $t_{2\downarrow}$ Co state, $[(Co^{2+}) \rightarrow (Co^+, h_{VB})]$. This process was suggested in Refs [13, 65, 66]. According to our results, the corresponding ionization energies are higher than 4 eV, which questions this interpretation.

We also point out that there are two recombination channels of photoelectrons, the direct recombination, and a two-step process in which the photoelectron is first captured by Co^{3+} , and then recombines via the internal $d-d$ transition.

The excitation-recombination processes are strongly affected by the intrashell Coulomb coupling. Manifestation of the coupling is provided by the pronounced dependence of the Co levels on their occupations. The levels of ionized Co^{3+} and $(Co^{3+})^*$ are lower than those of Co^{2+} due to the weaker intrashell Coulomb repulsion for an ion with smaller number of d -electrons. Additionally, both charge transfer transitions involve large lattice relaxations, which also influence the dopant levels. On the other hand, in spite of the fact the internal transition does not change the charge state, the Co^{2+} levels are shifted by about 1 eV. In this case, the effect has a different origin, namely the occupation-dependent $U(Co)$ corrections.

The theoretical level energies of Co depend on one parameter, $U(Co)$. Its value is established in two ways. First, we treat U as a fitting parameter. This allows us to reproduce the two measured ionization energies and the energy of the internal transition to within 0.1-0.2 eV with a single value $U(Co) = 3.0$ eV. Moreover, the discussed dependence of transition energies on U provides an additional insight into the impact of the + U corrections on the electronic structure of transition metal ions in semiconductors. In the second approach, the theoretical value $U(Co) = 3.4$ eV is obtained by the linear response method of Ref. [29]. It leads to somewhat less accurate energies of the optical transitions than the optimal fitted value 3.0 eV, but the agreement between the two methods is satisfactory. This further confirms our identification of the observed transitions. Those results demonstrate that GGA+ U is an alternative to the linear response time dependent density functional theory of Ref. [42].

ACKNOWLEDGEMENTS

The authors acknowledge the support from the Project No. 2016/21/D/ST3/03385, which are financed by Polish National Science Centre. Calculations were performed on ICM supercomputers of University of Warsaw (Grant No. G46-13 and G16-11).

-
- [1] Koidl P 1977 *Phys. Rev. B* **15**(5) 2493–2499
 - [2] Tuan A C, Bryan J D, Pakhomov A B, Shutthanandan V, Thevuthasan S, McCready D E, Gaspar D, Engelhard M H, Rogers J W, Krishnan K, Gamelin D R and Chambers S A 2004 *Phys. Rev. B* **70**(5) 054424
 - [3] Kim J H, Kim H, Kim D, Yoon S G and Choo W K 2004 *Solid State Commun.* **131** 677 – 680
 - [4] Pacuski W, Ferrand D, Cibert J, Deparis C, Gaj J A, Kossacki P and Morhain C 2006 *Phys. Rev. B* **73**(3) 035214
 - [5] Singh S, Rama N, Sethupathi K and Rao M S R 2008 *J. Appl. Phys.* **103** 07D108
 - [6] Gilliland S G, Sans J A, Sánchez-Royo J F, Almonacid G and Segura A 2010 *Appl. Phys. Lett.* **96** 241902
 - [7] Schulz H J and Thiede M 1987 *Phys. Rev. B* **35**(1) 18–34
 - [8] Jin Z W, Fukumura T, Hasegawa K, Yoo Y Z, Ando K, Sekiguchi T, Ahmet P, Chikyow T, Hasegawa T, Koinuma H and Kawasaki M 2002 *J. Cryst. Growth* **237-239** 548 – 552
 - [9] Matsui H and Tabata H 2013 *J. Appl. Phys.* **113** 183525
 - [10] Guo S, Li J and Du Z 2015 *Appl. Phys. A* **121** 645–649
 - [11] Xu J, Shi S, Li L, Zhang X, Wang J, Shi Q, Li S and Wang H 2013 *J. Electron. Mater.* **42** 3438

- [12] Renero-Lecuna C, Martn-Rodrguez R, Gonzlez J A, Rodrguez F, Almonacid G, Segura A, Muoz-Sanjos V, Gamelin D R and Valiente R 2014 *Chem. Mater.* **26** 1100–1107
- [13] Kittilstved K R, Liu W K and Gamelin D R 2006 *Nat. Mater.* **5** 291 – 297
- [14] Kumar S G and Rao K S R K 2015 *RSC Adv.* **5**(5) 3306–3351
- [15] Samadi M, Zirak M, Naseri A, Khorashadizade E and Moshfegh A Z 2016 *Thin Solid Films* **605** 2 – 19
- [16] Jaramillo T F, Baeck S H, Kleiman-Shwarscstein A, Choi K S, Stucky G D and McFarland E W 2005 *J. Comb. Chem.* **7** 264
- [17] Al-Salman H S and Abdullah M 2013 *J. Mater. Sci. Technol.* **29** 1139 – 1145
- [18] Jacob A A, Balakrishnan L, Shambavi K and Alex Z C 2017 *RSC Adv.* **7**(63) 39657–39665
- [19] Tseng L T, Suter A, Wang Y R, Xiang F X, Bian P, Ding X, Tseng A, Hu H L, Fan H M, Zheng R K, Wang X L, Salman Z, Prokscha T, Suzuki K, Liu R, Li S, Morenzoni E and Yi J B 2017 *Phys. Rev. B* **96**(10) 104423
- [20] Lu Z L, Hsu H S, Tzeng Y H, Zhang F M, Du Y W and Huang J C A 2009 *Appl. Phys. Lett.* **95** 102501
- [21] Ciatto G, Di Trolio A, Fonda E, Alippi P, Testa A M and Bonapasta A A 2011 *Phys. Rev. Lett.* **107**(12) 127206
- [22] Li L, Guo Y, Cui X Y, Zheng R, Ohtani K, Kong C, Ceguerra A V, Moody M P, Ye J D, Tan H H, Jagadish C, Liu H, Stampfl C, Ohno H, Ringer S P and Matsukura F 2012 *Phys. Rev. B* **85**(17) 174430
- [23] Dietl T, Andrearczyk T, Lipińska A, Kiecana M, Tay M and Wu Y 2007 *Phys. Rev. B* **76**(15) 155312
- [24] Sawicki M, Guziewicz E, Lukasiewicz M I, Proselkov O, Kowalik I A, Lisowski W, Dluzewski P, Wittlin A, Jaworski M, Wolska A, Paszkowicz W, Jakiela R, Witkowski B S, Wachnicki L, Klepka M T, Luque F J, Arvanitis D, Sobczak J W, Krawczyk M, Jablonski A, Stefanowicz W, Sztienkiel D, Godlewski M and Dietl T 2013 *Phys. Rev. B* **88**(8) 085204
- [25] Qi S, Jiang F, Fan J, Wu H, Zhang S B, Gehring G A, Zhang Z and Xu X 2011 *Phys. Rev. B* **84**(20) 205204
- [26] Spaldin N A 2004 *Phys. Rev. B* **69**(12) 125201
- [27] Walsh A, Da Silva J L F and Wei S H 2008 *Phys. Rev. Lett.* **100**(25) 256401
- [28] Gilliland S J, Sans J A, Sánchez-Royo J F, Almonacid G, García-Domene B, Segura A, Tobias G and Canadell E 2012 *Phys. Rev. B* **86**(15) 155203
- [29] Cococcioni M and de Gironcoli S 2005 *Phys. Rev. B* **71**(3) 035105
- [30] Gopal P and Spaldin N A 2006 *Phys. Rev. B* **74**(9) 094418
- [31] Chanier T, Virot F and Hayn R 2009 *Phys. Rev. B* **79**(20) 205204
- [32] Iuşan D, Knut R, Sanyal B, Karis O, Eriksson O, Coleman V A, Westin G, Wikberg J M and Svedlindh P 2008 *Phys. Rev. B* **78**(8) 085319
- [33] Sarsari I A, Pemmaraju C D, Salamati H and Sanvito S 2013 *Phys. Rev. B* **87**(24) 245118
- [34] Gluba M A and Nickel N H 2013 *Phys. Rev. B* **87**(8) 085204
- [35] Lany S, Raebiger H and Zunger A 2008 *Phys. Rev. B* **77**(24) 241201
- [36] Raebiger H, Lany S and Zunger A 2009 *Phys. Rev. B* **79**(16) 165202
- [37] Toyoda M, Akai H, Sato K and Katayama-Yoshida H 2006 *Physica B: Condens. Matter* **376-377** 647 – 650
- [38] Pemmaraju C D, Hanafin R, Archer T, Braun H B and Sanvito S 2008 *Phys. Rev. B* **78**(5) 054428
- [39] Patterson C H 2006 *Phys. Rev. B* **74**(14) 144432
- [40] Badaeva E, Feng Y, Gamelin D R and Li X 2008 *New J. Phys.* **10** 055013
- [41] Badaeva E, Isborn C M, Feng Y, Ochsenbein S T, Gamelin D R and Li X 2009 *J. Phys. Chem. C* **113**(20) 8710–8717
- [42] May J W, Ma J, Badaeva E and Li X 2014 *J. Phys. Chem. C* **118** 13152–13156
- [43] Hohenberg P and Kohn W 1964 *Phys. Rev.* **136**(3B) B864–B871
- [44] Kohn W and Sham L J 1965 *Phys. Rev.* **140**(4A) A1133–A1138
- [45] Perdew J P, Burke K and Ernzerhof M 1996 *Phys. Rev. Lett.* **77**(18) 3865–3868
- [46] Anisimov V I, Zaanen J and Andersen O K 1991 *Phys. Rev. B* **44**(3) 943–954
- [47] Anisimov V I, Solovyev I V, Korotin M A, Czyżyk M T and Sawatzky G A 1993 *Phys. Rev. B* **48**(23) 16929–16934
- [48] QUANTUM ESPRESSO, www.quantum-espresso.org
- [49] Karzel H, Potzel W, Köfferlein M, Schiessl W, Steiner M, Hiller U, Kalvius G M, Mitchell D W, Das T P, Blaha P, Schwarz K and Pasternak M P 1996 *Phys. Rev. B* **53**(17) 11425–11438
- [50] Özgür U, Alivov Y I, Liu C, Teke A, Reshchikov M A, Doğan S, Avrutin V, Cho S J and Morkoc H 2005 *J. Appl. Phys.* **98** 041301
- [51] Dong C L, Persson C, Vayssieres L, Augustsson A, Schmitt T, Mattesini M, Ahuja R, Chang C L and Guo J H 2004 *Phys. Rev. B* **70**(19) 195325
- [52] Izaki M and Omi T 1996 *Appl. Phys. Lett.* **68** 2439–2440
- [53] Srikant V and Clarke D R 1998 *J. Appl. Phys.* **83** 5447–5451
- [54] Lim L Y, Lany S, Chang Y J, Rotenberg E, Zunger A and Toney M F 2012 *Phys. Rev. B* **86**(23) 235113
- [55] Ciechan A, Przybylińska H, Bogusławski P, Suchocki A, Grochot A, Mycielski A, Skupiński P and Graszka K 2016 *Phys. Rev. B* **94**(16) 165143
- [56] Papierska J, Ciechan A, Bogusławski P, Boshta M, Gomma M M, Chikoidze E, Dumont Y, Drabińska A, Przybylińska H, Gardias A, Szczytko J, Twardowski A, Tokarczyk M, Kowalski G, Witkowski B, Sawicki K, Pacuski W, Nawrocki M and Suffczyński J 2016 *Phys. Rev. B* **94**(22) 224414
- [57] Ma X, Wu Y, Lv Y and Y Z 2013 *J. Phys. Chem. C* **117** 26029–26039
- [58] Calzolari A, Ruini A and Catellani A 2011 *J. Am. Chem. Soc.* **133** 5893–5899
- [59] Agapito L A, Curtarolo S and Buongiorno Nardelli M 2015 *Phys. Rev. X* **5**(1) 011006
- [60] Lany S and Zunger A 2008 *Phys. Rev. B* **78**(23) 235104
- [61] Lany S and Zunger A 2009 *Model. Simul. Mater. Sci. Eng.* **17** 084002
- [62] Komsa H P, Rantala T T and Pasquarello A 2012 *Phys. Rev. B* **86**(4) 045112
- [63] Ciechan A and Bogusławski P 2018 *Optical Materials* **79** 264 – 268
- [64] Liu W K, Salley G M and Gamelin D R 2005 *J. Phys. Chem. B* **109** 14486–14495

- [65] Johnson C A, Kaspar T C, Chambers S A, Salley G M and Gamelin D R 2010 *Phys. Rev. B* **81**(12) 125206
- [66] Johnson C A, Cohn A, Kaspar T, Chambers S A, Salley G M and Gamelin D R 2011 *Phys. Rev. B* **84**(12) 125203
- [67] Sanvito S and Pemmaraju C D 2009 *Phys. Rev. Lett.* **102**(15) 159701
- [68] Reynolds D C, Look D C, Jogai B, Litton C W, Cantwell G and Harsch W C 1999 *Phys. Rev. B* **60**(4) 2340–2344
- [69] More precisely, the multiple splitting of this line is not always resolved. Experimentally, the 2.0 eV line is split into two (1.88 and 1.92 eV [1], 2.02 and 2.18 eV [5]), three (1.88, 2.01, and 2.19 eV [3], 1.89, 2.04 and 2.19 eV [12], 1.9, 2.0 and 2.2 eV [11]), or even four peaks (1.89, 1.95, 2.06 and 2.19 eV [9], 1.91, 1.98, 2.09, and 2.18 eV [8]).
- [70] Lommens P, Smet P F, de Mello Donega C, Meijerink A, Piraux L, Michotte S, Mátéfi-Tempfli S, Poelman D and Hens Z 2006 *J. Lumin.* **118** 245 – 250